INTERNATIONAL JOURNAL OF REFRIGERATION 87 (2018) 47–64

Available online at www.sciencedirect.com

ScienceDirect

journal homepage: www.elsevier.com/locate/ijrefrig

Investigation into air distribution systems and thermal environment control in chilled food processing facilities

Demetris Parpas [a], *Carlos Amaris* [a,b,*], *Savvas A. Tassou* [a]

[a] *RCUK National Centre for Sustainable Energy Use in Food Chains (CSEF), Institute of Energy Futures, Brunel University London, Uxbridge, Middlesex UB8 3PH, UK*

[b] *Department of Energy, Universidad de la Costa, Cl. 58 #55-66, Barranquilla 080002, Colombia*

ARTICLE INFO

Article history:
Received 30 March 2017
Received in revised form 10 October 2017
Accepted 11 October 2017
Available online 19 October 2017

Keywords:
Air distribution systems
Temperature stratification
Refrigeration
Chilled food factories
Computational fluid dynamics (CFD)

ABSTRACT

Air flow distribution in chilled food facilities plays a critical role not only in maintaining the required food products temperature but also because of its impact on the facility energy consumption and CO_2 emissions. This paper presents an investigation of the thermal environment in existing food manufacturing facilities, with different air distribution systems including supply/return diffusers and fabric ducts, by means of both in-situ measurements and 3D CFD simulations.

Measurements and CFD simulations showed that the fabric duct provides a better environment in the processing area in terms of even and low air flow if compared to that with the diffusers. Moreover, temperature stratification was identified as a key factor to be improved to reduce the energy use for the space cooling. Further modelling proved that air temperature stratification improves by relocating the fabric ducts at a medium level. This resulted in a temperature gradient increase up to 4.1 °C in the unoccupied zone.

Enquête sur les systèmes de distribution d'air et la régulation de l'environnement thermique dans les installations de traitement des aliments réfrigérés

Mots clés : Système de distribution d'air ; Stratification de la température ; Froid ; Usines d'aliments réfrigérés ; Mécanique numérique des fluides (CFD)

* *Corresponding author.* Department of Energy, Universidad de la Costa, Cl. 58 #55-66, Barranquilla 080002, Colombia.
E-mail address: Carlos.amaris@outlook.com (C. Amaris).

https://doi.org/10.1016/j.ijrefrig.2017.10.019

Nomenclature

U	overall heat transfer coefficient [W·m^{-2}·K^{-1}]
R	thermal resistance [m^2·K·W^{-1}]
d	wall thickness (m)
q	thermal load per unit of area [W·m^{-2}]
T	temperature [°C]

Subscripts

i	overall
si	internal surface
se	external surface

Greek

ΔT	Temperature difference [°C]
λ	thermal conductivity [W.m^{-1}·K^{-1}]

1. Introduction

Chilled food chain relies heavily on refrigeration for the maintenance of low temperatures during processing, transportation and retail of chilled food products. In the UK, refrigeration systems in the cold food chain are estimated to be responsible for 16,100 GWh energy use and 13.7 MtCO2e Greenhouse Gas Emissions in 2010. These account for approximately 28% of final energy use and 7% of GHG emissions of the whole food chain for 2010 (Defra, 2012). In chilled food processing facilities, refrigeration can account for up to 60% of the total energy consumption of the facility. Chilled food processing takes place in large spaces with high ceilings where cooling is normally provided by ceiling mounted fan coil units, air-socks or diffusers. For the system to be effective, large air circulation rates and air velocities are required which, combined with the low temperatures, cause high energy consumption and in some cases discomfort for the workers in the space. Therefore, air distribution is an essential factor that needs to be carefully considered to create an environment capable of maintaining food quality and shelf life without excessive worker discomfort. The air distribution system should create a temperature and humidity homogeneity around the food product to maintain its quality and desired minimum shelf time. Mixing ventilation is the most commonly used air distribution method in chilled food processing environments. In a mixing ventilation system, air is mixed in the entire room volume which results in a fairly uniform environment in terms of temperature and contaminant concentration. In a chilled food facility with high ceiling height, the room volume that is needed to be conditioned is at the occupied space and where production takes place. Consequently, the usage of mixing ventilation systems in spaces with high ceilings can lead to energy wastage as this system tends to condition the whole air volume of the space.

The air distribution patterns in large spaces can be obtained from experimental tests including flow visualisation studies and from modelling approaches. Studies to date have focused on air distribution in large spaces in commercial buildings for ventilation and air conditioning applications to provide thermal comfort for the occupants and reduce energy consumption, and in cold rooms where the priorities are to maximise the holding volume and provide uniform temperatures in the space. Very little work has been reported in the literature on air distribution in chilled food factories where the objective is to maintain the temperature at low levels for food safety and quality at the expense of high energy consumption of the refrigeration plant. Therefore, improvement of the efficiency of the cold air temperature distribution in chilled food processing areas may play an important role to reduce the energy consumption of the facility.

Air flow modelling techniques such as Computational Fluid Dynamics (CFD) are becoming more popular over the last years since they provide a better understanding of air flow and temperature patterns in different situations in comparison with time-consuming and costly experimental tests. For instance, Moureh and Flick (2005) analysed the velocity characteristics throughout a long slot-ventilated enclosure considering different inlet flow arrangement. In this study, the author employed the high and low Reynolds number form of the two-equation k-ε model and the Reynolds stress model (RSM). According to the results, the RSM was able to predict correctly the general behaviour of primary and secondary air flow recirculation. Smale et al. (2006) reviewed CFD modelling applications for the prediction of air flow in refrigerated food storage applications. The k-ε turbulence model was found to be not accurate enough to be used in many refrigerated food storage applications, and only the Reynolds Stress Model (RSM) was found to predict the separation between the wall jets and the air flow patterns related to primary and secondary recirculation. Moureh et al. (2009a, 2009b) investigated the air flow patterns above and within an enclosure with vented boxes. The authors found that the RSM turbulence model represents reasonably the air ventilation levels values obtained by experimentation. Delele et al. (2009) applied multi-scale CFD model to predict air velocity, temperature and humidity distribution in a loaded cold room. They tested 4 different two-equation eddy-viscosity turbulence models to simulate the air velocities and compared the results against experimental measurements. Results showed that the standard k-ω/SST k-ω models provided better prediction accuracies of the air velocity. Later on, Ambaw et al. (2013) reviewed the application of CFD for the modelling of post-harvest refrigeration processes. The authors concluded that the RSM model was a more accurate model compared to the conventional k-ε, however, the k-ε model is more commonly used due to its lower computational requirements. Delele et al. (2013) also developed a three-dimensional (3D) model in CFD to predict air flow and heat transfer characteristics of a horticultural produce packaging system. The standard k-ε, RNG k-ε and standard k-ω two-equation turbulence models were considered and the SST k-ω was found to provide the most accurate predictions. Meanwhile, Duret et al. (2014) and Laguerre et al. (2015) created an empirical simplified model separated into zones for a cold room filled with food products. The simplified model was found to predict the product cooling rate and the final product temperature at different positions in the cold room quite well. For its part, Lin and Tsai (2014) studied the effect of supply diffuser position and supply air flow rate on the thermal environment of an indoor space. The authors reported that for

a given diffuser, the temperature gradient in the space reduces as the supply air flow increases due to greater mixing between the room and supply air.

Jurelionis et al. (2015) investigated the impact of the air supply method on the ventilation efficiency in a test chamber. In this investigation, results showed that the one-way mixing ventilation ceiling diffuser with low flow rate was more efficient in terms of ventilation in comparison with the four-way mixing and high air exchange rates. It was also concluded that the displacement air distribution method was less efficient than the mixing ventilation in terms of air removal. Rhee et al. (2015) evaluated the performance of an active chilled beam system in terms of uniformity for an indoor thermal environment in a full-scale test bed. The authors reported acceptable thermal uniformity with the active chilled beam system even at low air flow rates.

In general, CFD numerical studies applied to different refrigerated spaces for food conservation show that prediction of air velocity, temperature distribution and mean age of the air in these spaces can be obtained in good agreement with experimental data (Chanteloup and Mirade, 2009; Chourasia and Goswami, 2007a, 2007b, 2007c; Ho et al., 2010). Also, numerical studies involving stratified air temperature are also available for the performance analysis of underfloor air distribution systems (Fathollahzadeh et al., 2015; Pasut et al., 2014; Zhang et al., 2016), or for the optimization of thermal comfort and energy savings (Cheng et al., 2012, 2013; Ning et al., 2016). Lastly, Tassou et al. (2015) provided a review of modelling approaches of chilled spaces in the cold food chain.

Regarding the air distribution system location, studies from the open literature have shown that by modifying or relocating the air distribution system of different applications a significant improvement in the temperature distribution of the space can be achieved (Cheng et al., 2012, 2013; Ning et al., 2016). In addition, it has been observed that air distribution systems via displacement ventilation with different diffusers at a low level and metal based-slot diffusers at a medium level are not suitable due to nonhomogeneous and high air flows around the space (Parpas et al., 2015). In the case of chilled food manufacturing and processing facilities, an efficient air distribution configuration capable of cold air would lead to an energy consumption reduction in the refrigeration plant (Parpas et al., 2017a, 2017b). The key point for an existing chilled food production facility is to improve the efficiency of the air distribution systems with minimum changes on the actual system. Therefore, the improved air temperature distribution system should be adaptable from the existing system.

According to the literature, there are no studies evidencing air temperature distribution issues in chilled food processing facilities. Therefore, in the present study, an investigation of air distribution systems in two actual chilled food manufacturing facilities is presented. Data of temperature and velocities at different locations were collected from the two facilities to establish the thermal environment of the spaces. Two CFD 3D models were then developed based on the dimensions of the two processing food facilities. The models aim to predict the thermal environment of the two case studies and to allow reliable analysis of improved air distribution systems and their impact on the thermal environment of food processing areas.

2. Methods and facilities under investigation

The scope of this research aims to improve the cold air temperature distribution in chilled food processing areas. Improved air temperature distribution should lead to the reduction of the overall energy consumption of the refrigeration plant. Over the last decade, chilled food production facilities had the trend of using rooms with high ceilings. Usually, the unoccupied volume existing above 2 meters high in a cold room is the dead space in which chilled food products do not enter. As a result maintaining the unoccupied volume at a low temperature to provide chilled food safety is an energy waste. The first stage of this research focuses on understanding the air flow and the temperature variation in existing chilled food production facilities. Two 3D models based on CFD were developed for this purpose. Two existing chilled food production facilities (case study 1 and case study 2) using different air distribution systems were monitored. The monitoring of the facilities was implemented to understand the temperature and velocity distribution in the space and also to validate the CFD models. It is important to highlight that the two case studies are not presented for comparison purpose between them but to find out the air temperature distribution issues (such as high velocities, poor temperature distribution and cooling of the whole space) present in chilled food processing facilities where large spaces are used.

Temperature control in these facilities is achieved by cooling-coils operating with 100% of recirculated air and controlled by individual thermostats. Fresh air is supplied periodically in the space at room temperature without providing any contribution to the heat gains and cooling process. Therefore, fresh air is not considered in the modelling. The fresh air supply process in these facilities is very restricted to avoid contamination of the food and keep high standards of hygiene. In addition, to avoid any health problems in workers, it is known that the working time in these facilities is strictly limited.

The air temperature was measured using HOBO U12-013 type data loggers which were installed along the length at three different heights (knee level, head level and ceiling level) in the space. The data were logged every 5 minutes over a 14-day period. Air velocity and air dry-bulb temperature were also measured at the 3 different heights using a portable meter TSI TA465-P with a thermoanemometer articulated probe 966. Based on the type and the arrangement of the air distribution systems, for a better view and understanding of the air flow direction, measurements in two directions were applied (longwise and widthwise the facilities) for each measurement point. The logging interval of the instrument was set to 1 second and data were averaged over a period of 1 minute. Table 1 presents the measurement uncertainties of the sensors used.

2.1. *CFD models and solution procedure*

The steady-state 3D CFD models detailed in sections 2.2 and 2.3 were solved using the commercial ANSYS FLUENT® package (ANSYS FLUENT Theory Guide, 2011). The air inside the food processing area was considered to be compressible and the density was allowed to vary according to the ideal gas law to account for buoyancy effects. Other thermal properties were

Table 1 – Sensor and measurement uncertainties.

	Range	Uncertainty
Sensors		
HOBO – temperature sensor (°C)	0 to 50	± 0.35 °C
HOBO – RH sensor (%)	10 to 90	± 2.5%
Thermoanemometer – temperature sensor (°C)	–10 to 60	± 0.30 °C
Thermoanemometer – air flow meter ($m \cdot s^{-1}$)	0 to 50	± 3.0%
Thermoanemometer – RH sensor (%)	5 to 95	± 3.0%

maintained constant. The food was not considered in the simulations since it is already cold when it is sent (from a storage room at similar conditions to those in the processing facility) into the processing room. Besides, the time it stays in the room for processing and packing is very short so the effect that the heat gains from the food may have is negligible, therefore, it was neglected in the modelling.

The 3D models were solved using the SST k-ω model. The SST k-ω model has been pointed out in open literature as a more accurate model in comparison to the other k-ε and k- ω models (Delele et al., 2009, 2013; Stamou and Katsiris, 2006) and less time-consuming in comparison to the 7-equation Reynolds stress model.

The SST k-ω turbulence model is a two-equation eddy-viscosity model (Eqs. (1) and (3)) which was developed by Menter (1994) to effectively blend the robust and accurate formulation of the model in the near-wall region. In general, two-equation turbulence models allow the determination of the turbulent length and the time scale by solving two separate transport equations. The main difference from the turbulent viscosity definition of the standard k-ω turbulence model is that the modelling constants are different and is modified to take into account the transport of the turbulent shear stress. The SST k-ω turbulence model is more accurate and reliable for a wider class of flows than the standard k-ω model. The following transport equations define the SST k-ω turbulence model form.

$$\frac{\partial}{\partial t}(\rho k) + \frac{\partial}{\partial x_i}(\rho k u_i) = \frac{\partial}{\partial x_j}\left\{\Gamma_k \frac{\partial k}{\partial x_j}\right\} + \widetilde{G_k} - Y_k + S_k \quad (1)$$

$$\frac{\partial}{\partial t}(\rho \omega) + \frac{\partial}{\partial x_j}(\rho \omega u_j) = \frac{\partial}{\partial x_j}\left\{\Gamma_\omega \frac{\partial \omega}{\partial x_j}\right\} + G_\omega - Y_\omega + D_\omega + S_\omega \quad (2)$$

$$\widetilde{G_k} = \min(G_k, 10\rho\beta^* k\omega) \quad (3)$$

$$G_\omega = \frac{\alpha}{\upsilon_t}\widetilde{G_k} \quad (4)$$

In Eq. (1), $\widetilde{G_k}$ represents the generation of turbulence kinetic energy due to mean velocity gradients. In addition, in Eq. (2) G_ω represents the generation of ω which is calculated likewise the standard k-ω turbulence model. Γ_k and Γ_ω represent the effective diffusivity of k and ω respectively. Y_k and Y_ω represent the dissipation of k and ω due to turbulence. D_ω is the cross-diffusion term, and S_k and S_ω are user-defined source terms. $\widetilde{G_k}$ and G_ω are estimated as shown in Eqs. (3) and (4), respectively. In Eq. (3) G_k is determined as in the standard k-ω model. α is a factor for turbulent viscosity causing a low Reynolds number correction.

The effective diffusivities Γ_k and Γ_ω are determined by Eqs. (5) and (6). σ_k and σ_ω are the turbulent Prandtl numbers for k and ω, respectively. μ_t refers to the turbulent viscosity. More details of the turbulence model can be found in the references (ANSYS FLUENT Theory Guide, 2011; Menter, 1994).

$$\Gamma_k = \mu + \frac{\mu_t}{\sigma_k} \quad (5)$$

$$\Gamma_\omega = \mu + \frac{\mu_t}{\sigma_\omega} \quad (6)$$

Each 3D model was solved with the pressure based solution algorithm, second order upwind energy and momentum discretisation, body-force-weighted pressure discretisation, and SIMPLE pressure-velocity coupling. The second order upwind scheme is using a multidimensional linear reconstruction approach to compute with better accuracy the quantities at cell faces. In addition, the body-force-weighted scheme implements the face pressure computations with the assumption that the normal gradient of the difference between pressure and body forces is constant. The SIMPLE pressure-velocity coupling uses a relationship between velocity and pressure corrections to enforce mass conservation and to obtain the pressure field. More details about how CFD fluent works can be found in the ANSYS Fluent Theory Guide (2011). The air inside the food processing area was considered to be compressible and the density was allowed to vary according to the ideal gas law to account for buoyancy effects. Other thermal properties were maintained constant (specific heat, thermal conductivity and viscosity). The raw materials of the food products were not considered in the simulation boundary conditions. The majority of the raw materials are already cooled down prior to their entry into the processing lines. Hence, any effect that the heat gains from the food raw material thermal mass may have to the thermal environment is negligible; therefore, it was neglected in the modelling.

2.2. *Case study 1: Air distribution via supply/return diffusers*

The dimensions of the case study 1 chilled food processing area under investigation are 17 m wide, 40 m deep and 4 m high. Fig. 1a shows a plan view of the facility including the space geometry of case study 1. The HVAC system consists of 4 individually controlled Air Handling Units (AHU) in the roof void, supplying air to the room space through 4 diffusers, one per AHU. The location of the diffusers on the ceiling and measurement points are also shown in Fig. 1a. In addition, the horizontal black lines in Fig. 1a indicate the production lines locations over the facility. The arrows indicate the diffusers fins which were adjusted by the occupants. The portable meter was used in the data collection. The data were logged at 3 different heights (ceiling, head and knee level) and two different directions for each measurement point. The diffusers

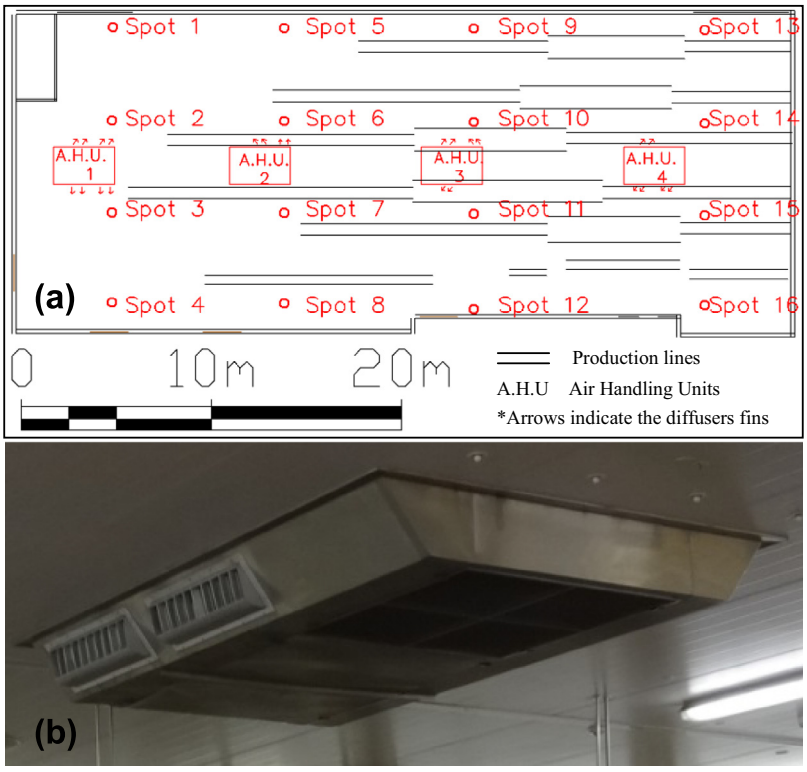

Fig. 1 – Case study 1, (a) planar view of the model geometry and measurement points and (b) air distribution system via supply/return diffusers.

are combined supply/return diffusers (Fig. 1) and supply air from two sides along the width of the space and air is returned through a return grille at the bottom face of the diffuser. The thermostats, which are located on the return duct, were set to 10 °C. The air cooling units operate 24 hours per day and the air supply from each unit to the room space is approximately 1.4 $m^3 \cdot s^{-1}$. The maximum occupancy density of the space is 110 people.

2.2.1. *Model boundary conditions*

Case study 1 model was designed using the actual dimensions of the chilled food processing area as shown in Fig. 1 and Fig. 2. The supply and return air flows from each air handling unit were set to a value of 1.4 $m^3 \cdot s^{-1}$. The air supply and return air diffuser boundary conditions were defined as mass flow inlets and outlets, respectively. The air supply temperature was set at 7 °C. The occupancy density was set to be the maximum of 110 occupants. The occupants' positions are indicated in Fig. 2 which are placed to both sides of the production lines. This occupant arrangement occurs during peak production. Each occupant was defined as a parallelepiped box with a surface area of 1.84 m^2 (X: 0.1, Y: 1.8, Z: 0.4) and thermal load of 105 $W \cdot m^{-2}$. The occupant's thermal load was defined by the state of activity (typical metabolic heat generation) based on ASHRAE suggestions (ASHRAE, 2013). The lighting thermal boundary condition was defined with a temperature of 28 °C for all the lights surfaces (value measured experimentally). The production line motors were defined as surfaces with a temperature of 105 °C (measured experimentally). The motors are placed at the beginning and end of each production line. In total 12 motors are placed in the model. Other heat sources in the processing area were neglected for this phase of the research. The surrounding walls were considered adiabatic since the adjoining spaces operate at similar conditions. The thermal boundary conditions of the ceiling and floor were defined as thermal heat flux values calculated by taking into account the temperature profile and thermal resistances (Eqs. (7–9)) over the interior and exterior of the construction.

$$Ui = \frac{1}{Rsi + R1 + Rse}\left(\frac{W}{m^2K}\right) \tag{7}$$

$$R1 = \frac{d}{\lambda}\left(\frac{m^2K}{W}\right) \tag{8}$$

$$q = Ui \times \Delta T\left(\frac{W}{m^2}\right) \tag{9}$$

In Eq. (7), *Ui* represents the overall heat transfer coefficient and in Eq. (8), *R1* represents the thermal resistance per unit area of the construction; *d* represents the thickness and λ the thermal conductivity of the construction. In Eq. (7), *Rsi* and *Rse* represent the outside and inside surface resistances respectively (values are defined by the direction of the heat flow). In Eq. (5), *q* represents the total heat flow per unit area of the construction. The floor heat flux was calculated assuming a suggested ground temperature of 10.8 °C (value suggested for London by CIBSE, 2015) and an insulated floor with a thermal conductivity of 0.5 $W \cdot m^{-1} \cdot k^{-1}$. In the case of the ceiling boundary, an adjoining space temperature of 20 °C was assumed, and

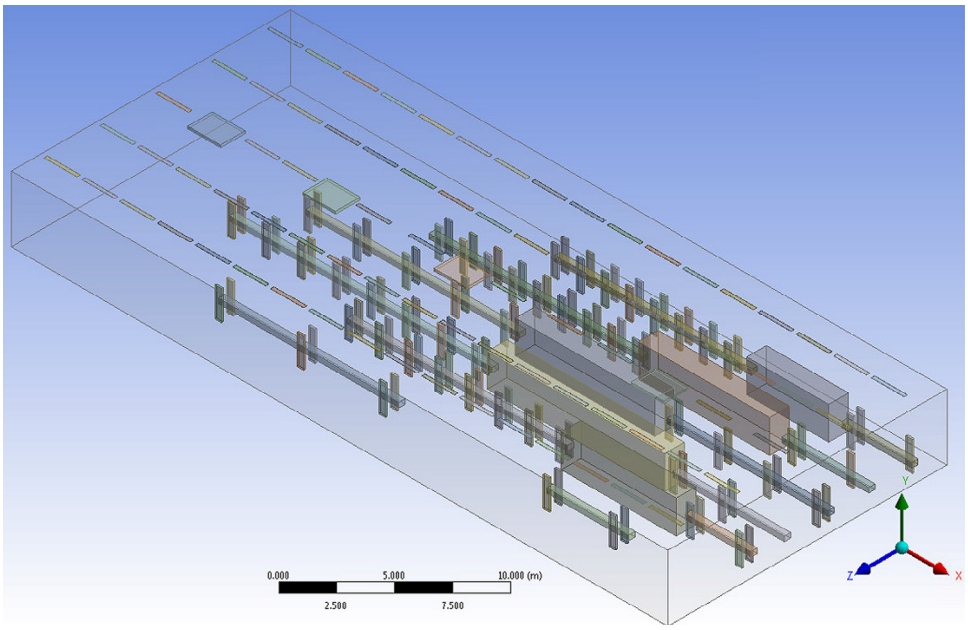

Fig. 2 – Case study 1, 3D model.

the ceiling was made of sandwich panels with heat transfer coefficient of 0.28 $W \cdot m^{-2} \cdot k^{-1}$.

The computational domain was discretised with an automatic mesh method, mainly with tetrahedral and hexahedral cells generated using the built-in ANSYS design modeller meshing algorithm. The resulting mesh consisted of hexahedral cells at the near-wall layers/domain and with tetrahedral and hexahedral cells in the air domain. The mesh density was gradually refined near the building wall, internal heat gains surfaces and the air handling unit supply/return diffusers. The final mesh size consists of 32 million elements, with element dimensions between 0.04–0.15 m. Four inflation layers were employed near the wall surfaces with a first element size of 0.1 m and a growth ratio of 1.2. In addition, a finer mesh was applied by four inflation layers near the internal heat gain surfaces (occupants and lighting) and the air supply/return diffusers with a first element size of 0.4 m and a growth ratio of 1.2 to capture the effects of the boundary layer. The mesh gradually increases towards the bulk of the air domain producing a maximum element size of 0.15 m.

The final model mesh was generated following a mesh independence study. The convergence criteria for the independence study were set to reach at least a 10^{-5} residual error for continuity and an average temperature tolerance of ±0.5 °C. Mesh refinement was performed by varying all mesh sizes by the same ratio, but maintaining the inflation parameters. The simulation time for each steady-state case was 48 hours, with an average of 1500 iterations, on a 2.6 GHz, 32 GB RAM, Intel Xeon Processor with 12 parallel threads. Simulation results on the mesh independent grid showed an average y^+ value of 6.

2.3. *Case study 2: Air distribution via fabric ducts*

The dimensions of the case study 2 chilled food processing area under investigation are 21 m wide, 24 m deep and 6.5 m high. Fig. 3a shows the space geometry of case study 2. The HVAC system consists of 5 evaporator coils (E#) distributing the air with fabric ducts with a diameter of 0.9 m located at 6.0 m height, Fig. 3b.

More details about the fabric duct can be found in Ke-fibertec KE. The temperature in this facility is controlled by individual thermostats located at the back of each evaporator with 8–9 °C air of set point temperature. The location of the evaporators is also shown in Fig. 3a. The air flow rate that is recirculated from each evaporator is approximately 4.5 $m^3 \cdot s^{-1}$. The maximum occupancy density of the space is 96 people. Red circles in Fig. 3a show the points where the Hobos data loggers were located. The data loggers were installed at 3 different height levels for each measuring point.

2.3.1. *Model boundary conditions*

The case study 2 3D CFD model was designed using the actual dimensions of the chilled food processing area, Fig. 4. The supply and return air flow from each evaporator were set at 4.5 $m^3 \cdot s^{-1}$. The target in an air-sock is to achieve a constant static pressure inside the sock which will maintain its inflation and will give a uniform discharge air velocity across the whole surface (normally around 0.1 $m \cdot s^{-1}$). The discharge air surface velocity is too low to give a momentum to the air to be thrown into the space. Due to the density difference between the supplied air and the room air, the supply air is displaced towards the floor immediately after passing through the sock surface. For the CFD modelling boundary conditions, the air supply from the air-socks was defined as mass flow inlet setting up the total coil air volume. The modelling air-sock surface discharge air velocity varied around 0.1 and 0.2 $m \cdot s^{-1}$. In addition, the coil return air boundary conditions were defined as mass flow outlets. The air supply temperature was set at 7 °C. The occupancy density was set to be the maximum of 96 occupants. Each occupant was defined as a parallelepiped box with a surface area of 1.84 m^2 (X: 0.1, Y: 1.8, Z: 0.4) and thermal load

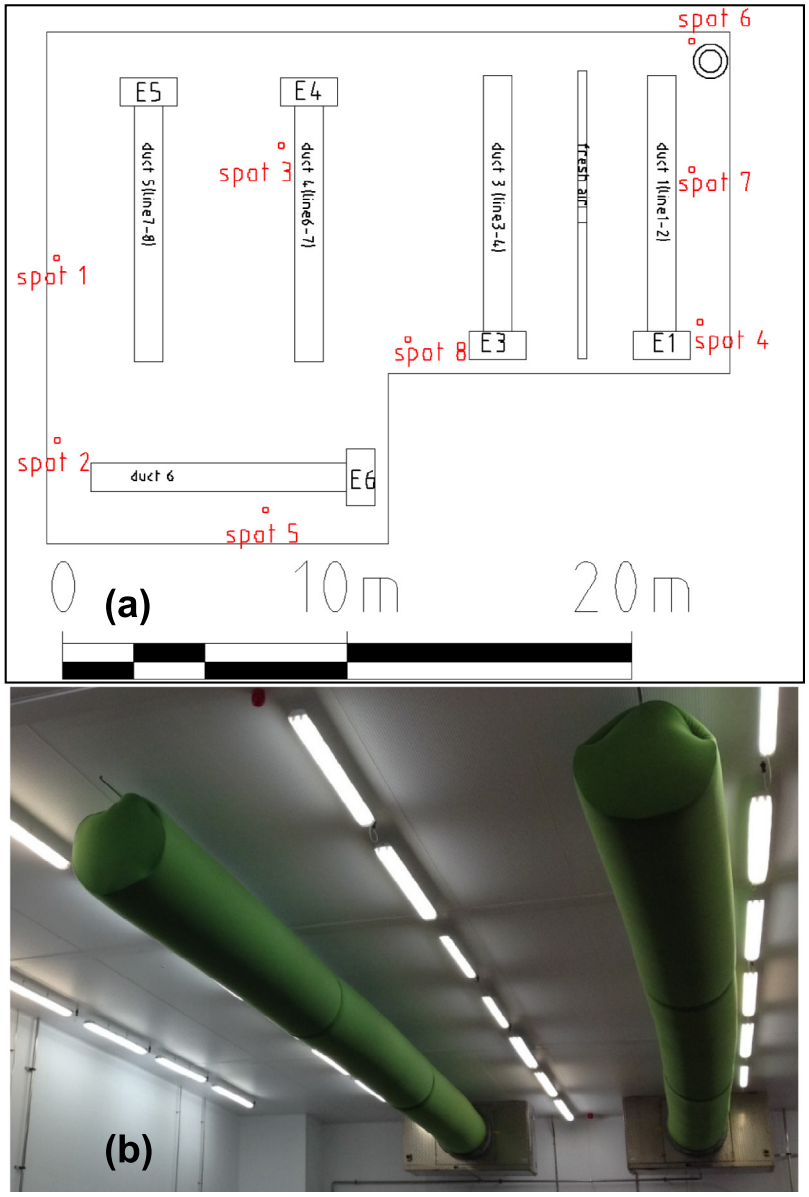

Fig. 3 – Case study 2, (a) planar view of the model geometry and measurement points and (b) air distribution system via fabric ducts.

of 105 $W{\cdot}m^{-2}$. The occupant's thermal load was defined by the state of activity (typical metabolic heat generation) based on ASHRAE suggestions (ASHRAE, 2013). The lighting thermal boundary condition was defined with a temperature of 28 °C for all the lights surfaces. Other heat sources in the processing area were neglected. The surrounding walls were considered adiabatic since the adjoining spaces operate at similar conditions. The floor heat flux boundary condition was calculated taking into account a ground temperature of 10.8 °C (suggested annual average outside temperature in London, CIBSE, 2015) and an insulated floor with a conductivity of 0.5 $W{\cdot}m^{-1}{\cdot}k^{-1}$. The ceiling boundary was established with an adjoining space temperature of 20 °C, and the ceiling made of sandwich panels with heat transfer coefficient of 0.28 $W{\cdot}m^{-2}{\cdot}k^{-1}$.

The computational domain was discretised with an automatic mesh method, mainly with tetrahedral and hexahedral cells generated using the built-in ANSYS design modeller meshing algorithm. The mesh density was gradually refined near the building wall, internal heat gains surfaces and the air-socks. The final mesh size consists of 34 million elements, with element dimensions between 0.04–0.1 m. Four inflation layers were employed near the wall surfaces with a first element size of 0.08 m and a growth ratio of 1.2. In addition, a finer mesh was applied by four inflation layers near the internal heat gain surfaces (occupants and lighting) and the air-socks with a first element size of 0.4 m and a growth ratio of 1.2 to capture the effects of the boundary layer. The mesh gradually increases towards the bulk of the air domain producing a maximum element size of 0.1 m. The final model mesh was generated following a mesh independence study. The convergence criteria for the independence study were set to reach at least a 10^{-5} residual error for continuity and an average temperature

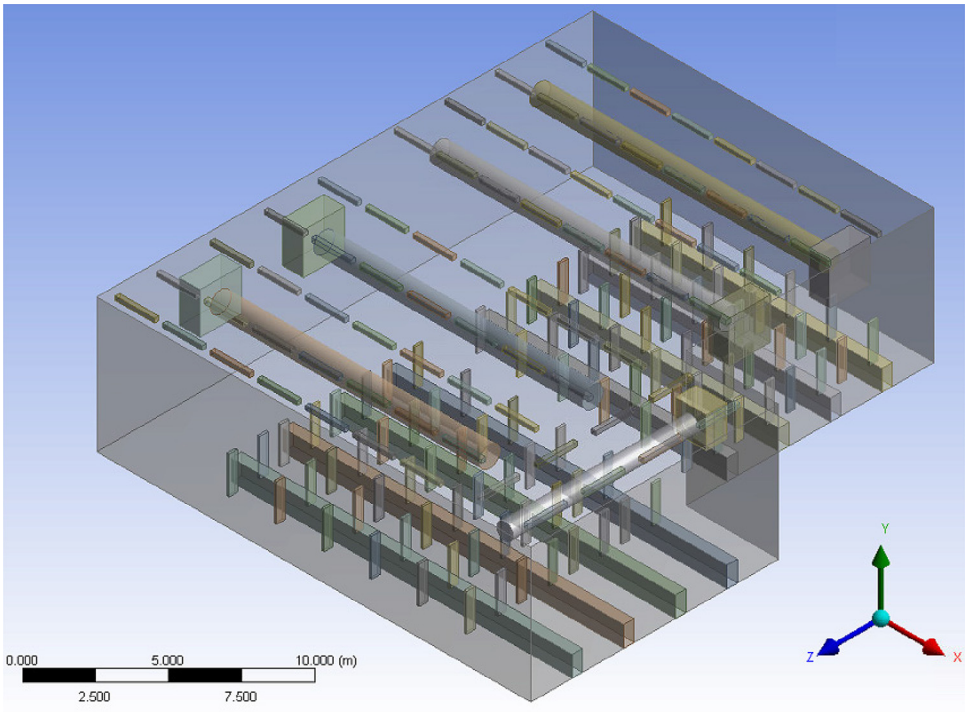

Fig. 4 – Case study 2, 3D model.

tolerance of ±0.5 °C. Mesh refinement was performed by varying all mesh sizes by the same ratio, but maintaining the inflation parameters. The simulation time for each steady-state case was 48 hours, with an average of 3000 iterations, on a 2.5 GHz (2 processors), 64 GB RAM, Intel Xeon Processor with 38 parallel threads.

3. Results and discussion

This section presents an analysis of the thermal environment in terms of air flow and temperature of the two processing food facilities. CFD simulation results for each facility case study are also presented and compared with the measured data. Finally, the developed CFD model is used to improve the temperature stratification in one of the case studies presented.

3.1. *Measurements, case study 1 and 2*

The temperature and velocity variations over the space of the case study 1 facility can be observed in Fig. 5. In Fig. 5 it can be noted that the average air temperature in the space varied between 11.5 and 14.0 °C with a ±0.5 °C variation in each point of measurement while air velocities ranged between 0.1 and 1.4 $m \cdot s^{-1}$. According to the recorded data shown in Fig. 5, the vertical temperature gradients around the space are insignificant. Also, temperatures measured at the different points in horizontal direction showed similar values. This means that the air distribution configuration via supply/return diffusers cools down the whole space including a large unoccupied volume.

Regarding the air flow velocities around the space shown in Fig. 5, the highest values were obtained at the ceiling level and the lowest values at the head and knee level. Air velocities in each point of measurement were found to vary up to ±0.3 $m \cdot s^{-1}$. At head level, the velocity in some locations was as high as 0.6 $m \cdot s^{-1}$ which, together with the low temperatures, can lead to excessive percentage dissatisfied discomfort up to 60% or higher for the occupants according to the BS EN ISO 7730 (2005).

According to the measurements, it can be said that the air distribution system via supply/return diffusers is effective to keep the required conditions of temperature around the production lines, and therefore to maintain the quality of the food during its processing. However, it can be said that this air distribution configuration provides poor temperature stratification which was observed in the whole space of the facility if compared with an air distribution system capable of localizing the cold where it is needed.

Fig. 6 shows the temperature and velocity trends over the space for case study 2. In contrast to case study 1, monitoring of the case study 2 facility showed some temperature stratification, with the lowest temperatures measured at knee level and highest at ceiling level. With a supply temperature from the air-socks at 7 °C, the average temperature in the bulk of the space varied between 9.0 and 13.5 °C with a ±0.5 °C variation in each point of measurement. It was also observed that the temperature stratification between the three measuring heights followed an apparent steady distribution pattern. However, it should be noted that most of the sensors were located close to the facility walls which implies that temperature stratification may occur mainly close to the walls.

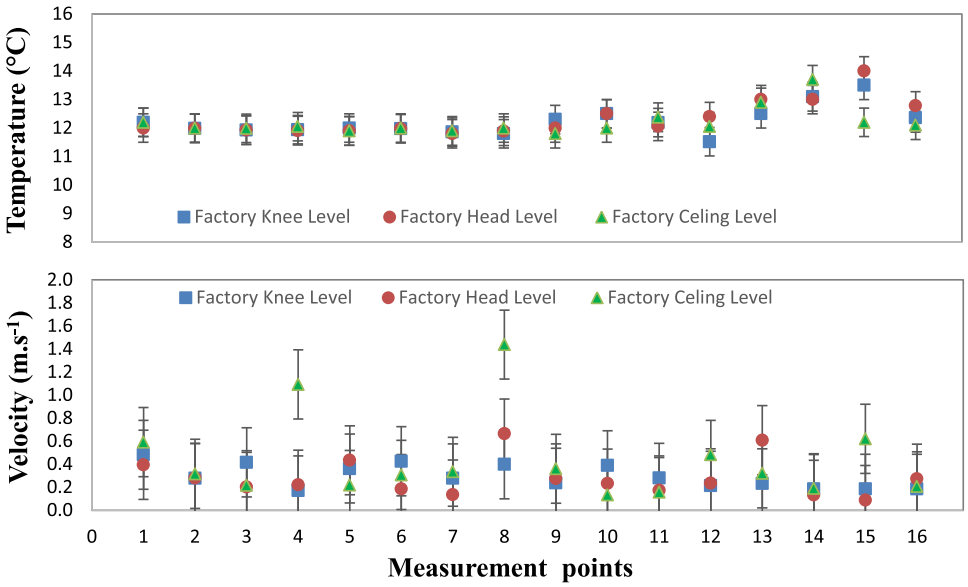

Fig. 5 – Case study 1, air temperature and velocity measurements.

In addition, in Fig. 6 the point of measurement 3 also shows that in the case of the zones close to the air distribution systems the temperature stratification may be just slight. With regards to the air flow velocities in case study 2, they were found to vary between 0.05 and 0.15 $m \cdot s^{-1}$ with a variation up to ± 0.1 $m \cdot s^{-1}$ and the highest velocities measured at the knee and head level. Measurements show that air velocities in case 2 were much lower than those in case 1 resulting in a beneficial effect to achieve a partial temperature stratification in the space with low air velocities.

Based on the measured data, the use of fabric ducts appears to be a more appropriate configuration for air distribution in comparison to that in case 1. Fabric ducts employ wider air flow areas covering the production lines and distributing low air flow velocities around the occupied zone. It also seems to facilitate the air temperature stratification around those spaces that are not directly cooled by the air flows from the air distribution system.

3.2. *Case study 1 modelling*

This subsection shows the results from the modelling of the facility with air distribution via supply/return diffusers. Fig. 7 shows the air temperature distribution at 5 lateral sections

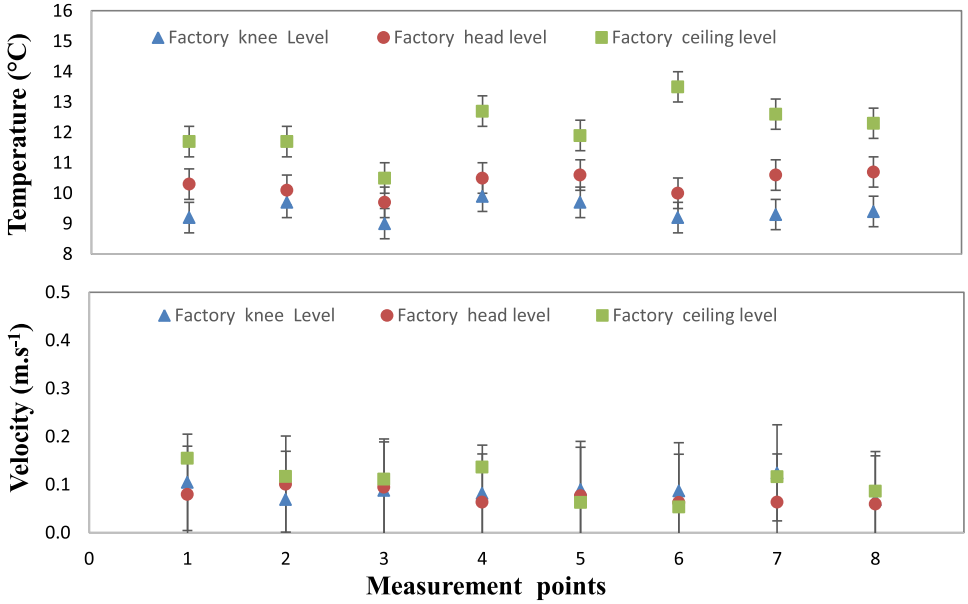

Fig. 6 – Case study 2, air temperature and velocity measurements.

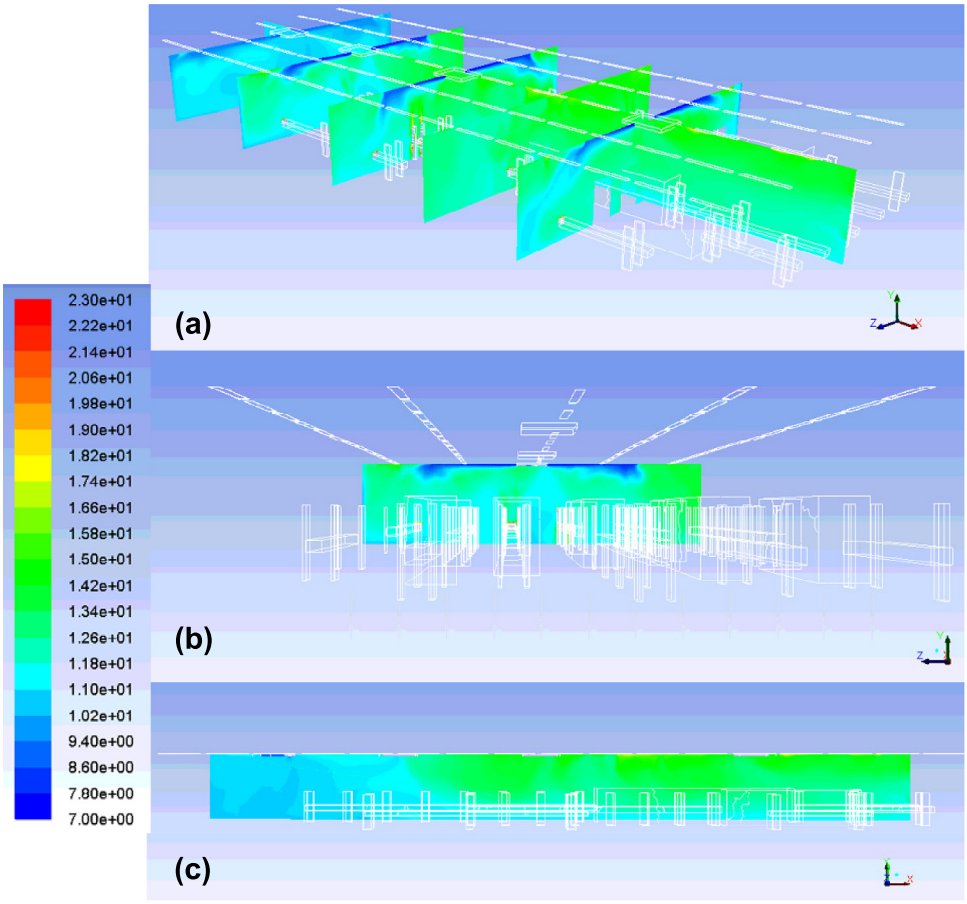

Fig. 7 – Case study 1, CFD modelling of air temperature in the space (°C), (a) 3D view, (b) frontal view, and (c) side view.

along each diffuser and a longitudinal section along the centre line of the space. With a supply temperature from the diffusers at 7 °C the temperature in the bulk of the space varied between of 10.4 °C and 13.2 °C considering the same measurement points as in Fig. 1a. As seen in Fig. 7 temperature modelling showed just a small temperature stratification around the space. In addition, it can be observed that the lowest temperatures were reached at ceiling level and close to the walls. On the other hand, temperatures slightly higher were found around the occupied zone which may be the result of the heat gains from the occupants. These results agree with the data collected from the measurements which also showed a poor stratification around the space of the food processing facility.

In addition, Fig. 8 shows the modelled velocity distribution at 5 cross sections from each supply diffuser. According to the modelling results, the air velocity around the whole space varied between 0.05 and 1.6 $m \cdot s^{-1}$. The highest air velocities were mainly obtained at the ceiling level as it could be expected due the diffusers small area used for the air distribution. It can also be observed that the flow patterns are not as homogeneous over the space as required and that air velocities are also relatively high close to walls. With this air distribution configuration, the air flows along the ceiling to the side walls, and then it flows down the wall until it reaches the floor. Then, recirculation takes place in an area between floor level and 2.5 m above floor level. There is also some air recirculation between the supply and return grilles sections of the combined supply/return diffusers which imply an inefficient use of supply cold air. In Fig. 8 it can also be noted that the air displacement around the space is mainly influenced by the high air flow velocity from the supply/return diffusers rather than buoyancy effects due to heat gains from the workers and equipment. Modelling results confirm that this type of air distribution system tends to cool down almost uniformly the whole volume of the space at very high and nonhomogeneous air flow velocities.

Fig. 9a presents a comparison between the average temperature data collected including the measurement uncertainty and the modelling results. The position of each point of measurement can be identified in Fig. 1. From Fig. 9a it can be observed that predicted air temperatures are lower than the measured data. In the case of the CDF model for the case study 1, it was developed for fixed fins supply diffusers. However, the case study 1 chilled food facility supply diffusers have adjustable fins that are manipulated by the workers. As a result of the occupant's on-site fins adjustment, it could have resulted in an even more homogeneous space temperature which was the reason why modelling results showed slightly lower temperatures at a low level and higher temperatures at ceiling level compared with experimental measurements. However, the model shows a good level of prediction for the air temperature trend and distribution achieved in this case study in

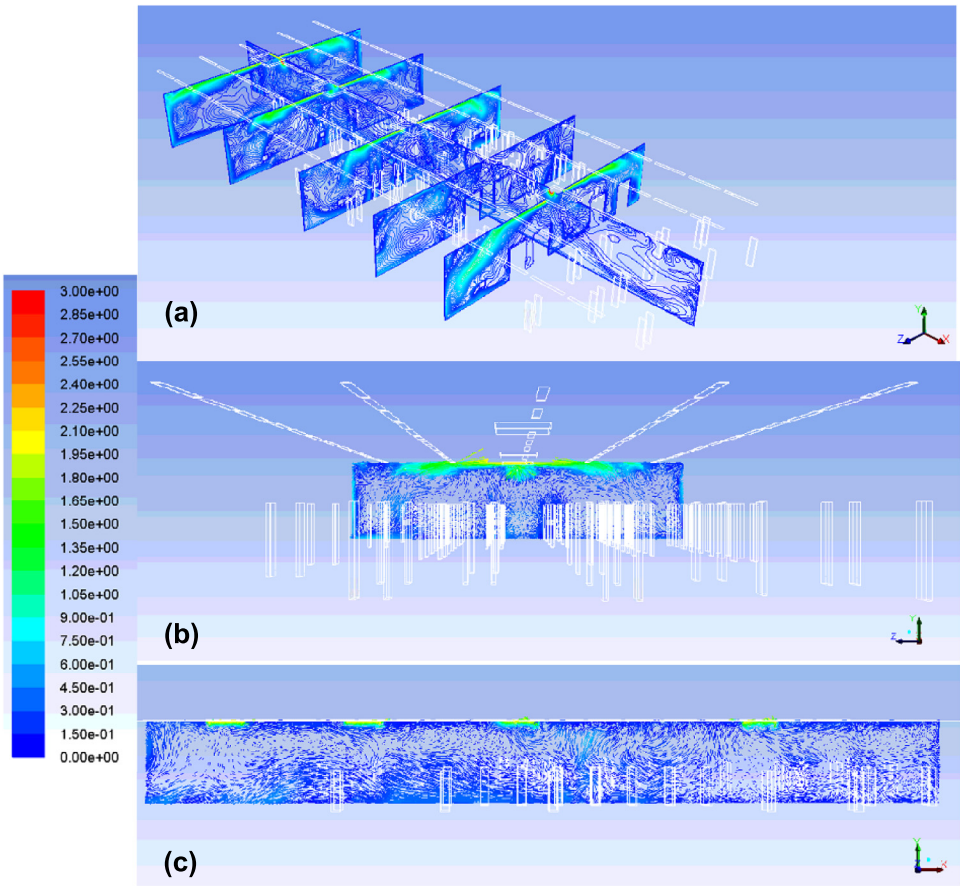

Fig. 8 – Case study 1, CFD modelling of air velocity in the space (m·s^{-1}),(a) 3D view, (b) frontal view, and (c) side view.

which very poor temperature stratification in the space was observed.

To determine the validity of the model, the temperature profiles predicted by the model were compared against temperature measurements in the space. Results from this comparison are shown in Fig. 9b. To conclude to the maximum error boundaries (+2.0 °C and –1.8 °C error), for each measurement spot all modelling values were subtracted from experimental values. The middle line in the graph indicates the position of 0 °C error.

The line above and below indicates the error boundaries of +2.0 °C and –2.0 °C. The blue spots indicate the modelling values on X axis and experimental value on Y axis. The distance from the red line depicts the prediction error. Blue spots existing above and below the red line presents a positive and negative prediction error respectively. The absolute average error across all test points in the space was found to be 0.8 °C lower than the measured values. The formula used to calculate the absolute error is given in Eq. (10). The maximum absolute error was found to be 2.0 °C higher than the measured value.

$$\text{Absolute Error} = \text{CFD Value-Experimental Value} \quad (10)$$

3.3. *Case study 2 modelling*

Modelling results of the facility with air distribution via fabric ducts are presented below. Fig. 10 presents the modelled air temperature distribution at different cross sections along the space. With a supply temperature from the air-socks at 7 °C the temperature in the bulk of the space varied between of 9.5 and 12.6 °C considering the same measurement points in Fig. 3a. From all air temperatures values measured at each point, the lowest temperature values were obtained at knee level and the highest temperatures at ceiling level. Temperature modelling confirms that a slight stratification was obtained as it was also the case for the measured data especially at those measurement points close to the facility walls. Furthermore, Fig. 10b and c shows that the space below the fabric ducts and above head level present even lower air temperatures than those between head level and knee level. It confirms that there is an insignificant temperature stratification around the zones directly below fabric ducts due to the low temperature of the air supplied. This agrees with the measurements (see Fig. 6) due to the fact that, for instance, the point of measurement 3 being located below fabric 4 showed just a small air temperature gradient if compared to those at the other measurement points. In addition, Fig. 10 shows that the air temperature between head level and knee level around the production lines is influenced by the heat gains from the workers.

Fig. 11 depicts the modelled air velocity distribution at different cross sections along the space. In this figure it can be observed that air velocities at the different measurement points (Fig. 3) were very low and ranged from 0.02 to 0.25 m·s^{-1}.

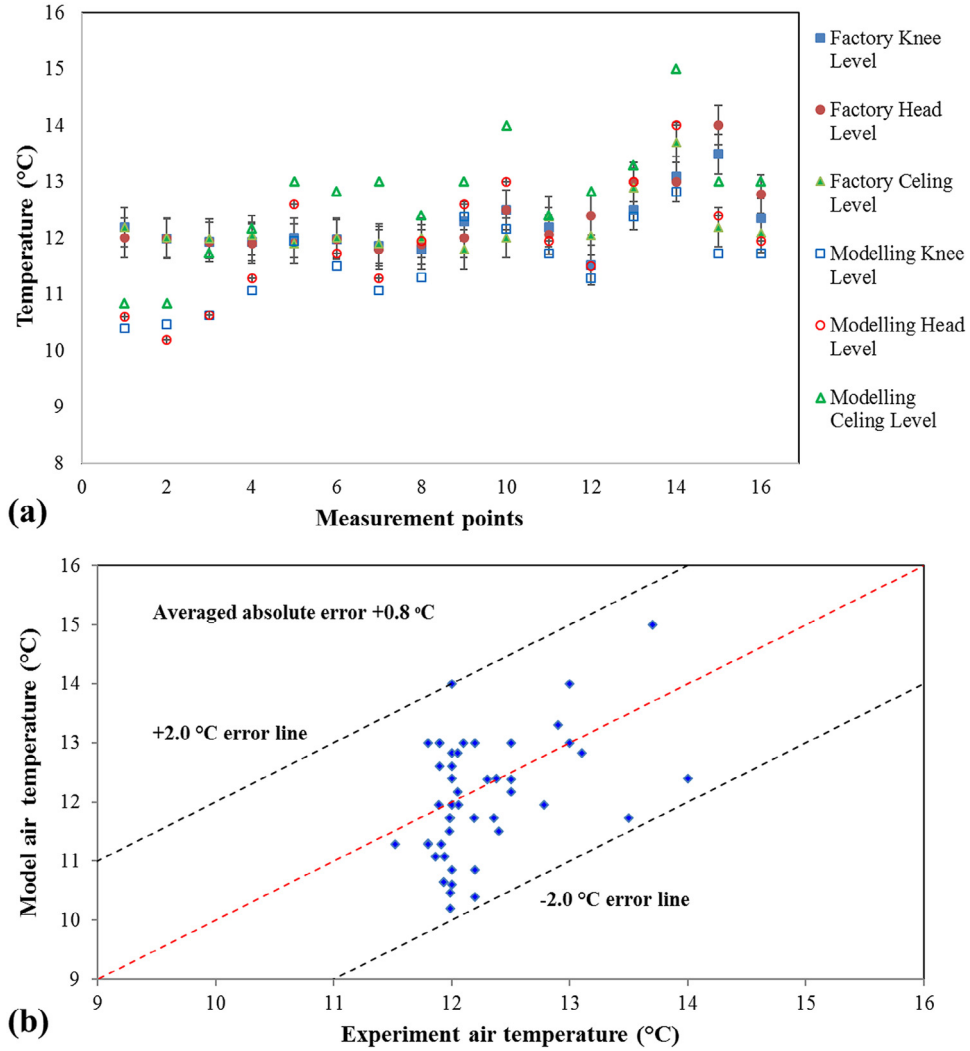

Fig. 9 – Case study 1, (a) air temperature uncertainty analysis and (b) CFD modelling air temperature valuation. (For interpretation of the references to colour in this figure, the reader is referred to the web version of this article.)

Moreover, modelling results also show that higher values can be found close to the evaporator air return and along the workers. From the simulation it can also be noted that the direction of the air flow is influenced mainly by the suction from the evaporator coils located at different points of the facility and in a lesser extent due to buoyancy effects from the worker's heat gains.

It is then observed that the use of fabric ducts for air distribution allows having an even and low air flow distribution over the production zone which is at some extent beneficial for the workers. Fig. 12a and b presents the comparison between the average temperature data collected including the measurement uncertainty and the modelling results. This figure also shows that the model underpredicts the air temperatures in comparison to the measured data, however, the model shows a better level of prediction for the air temperature distribution in comparison with that of the case study 1. The average absolute error across all test points in the space was found to be 0.6 °C lower than the measured values. The maximum error was found to be 1.7 °C lower than the measured value. In any case, predicted air temperatures also show some level of stratification just as observed from the measured data.

The modelling results validation shows that the predicted air temperatures and their trends are in good agreement with the data collected from the two facilities with different air distribution systems. Furthermore, based on the measurements and modelling results, it can be highlighted that fabric ducts provide a better environment in the space in terms of air velocity uniformity at the level of the production area in comparison to the use of air supply/return diffusers. In addition, temperature stratification can be improved by relocating the fabric duct in a way that the cold air is localised around the production zone to reduce the energy use for the cooling of the whole space.

3.4. *Improved temperature distribution*

This section presents the results from the modelling of case study 2 with the air distribution system via fabric ducts located at a medium level. The fabric duct was selected due to the following reasons: wide air flow area which results in low air

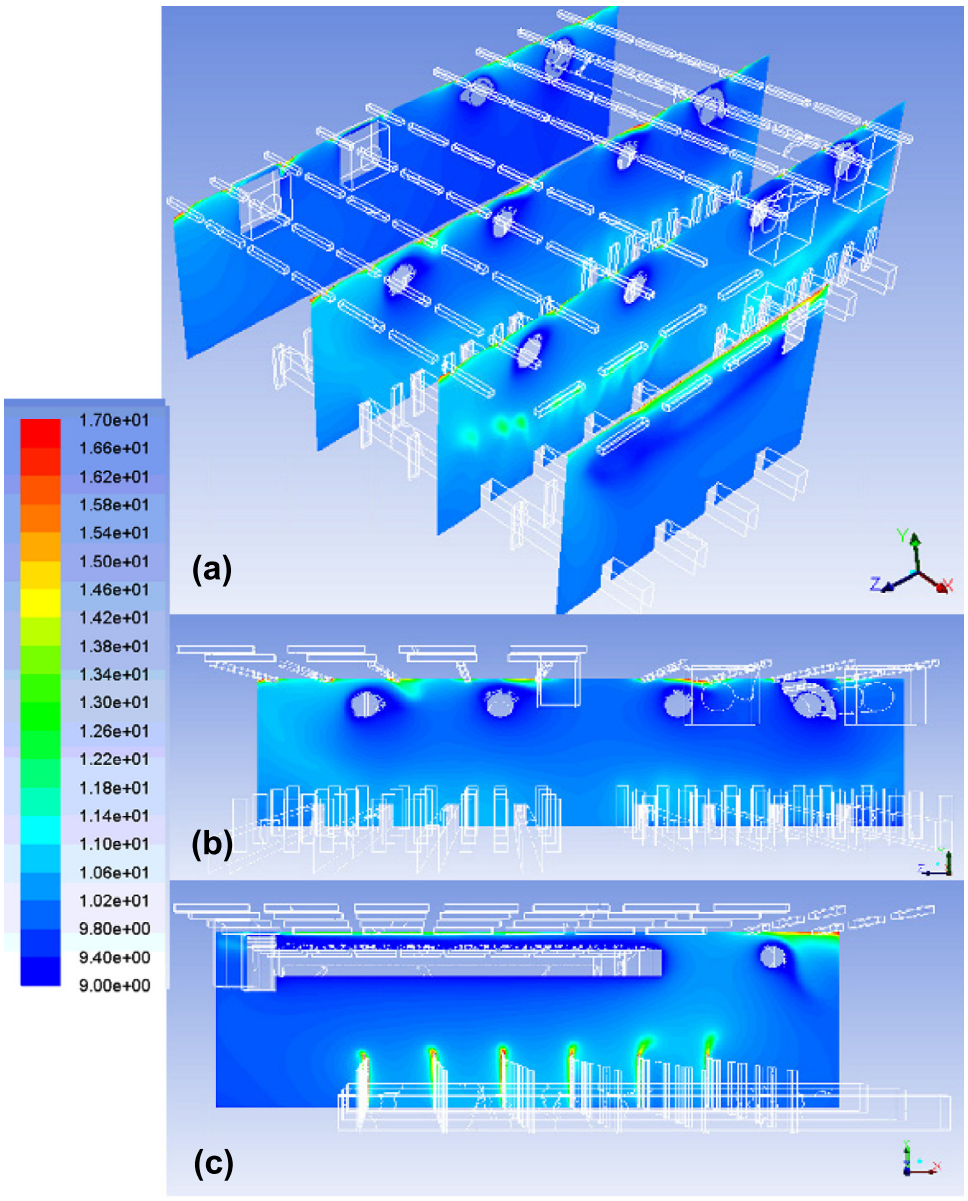

Fig. 10 – Case study 2, CFD modelling of air temperature in the space (°C), (a) 3D view, (b) frontal view, and (c) side view.

velocities, homogeneous air flow distribution over the production zone and easy adaptability. The 3D CFD model was implemented with the same boundary conditions and solution procedure as those in the initial model. The main difference with respect to the reference case is that the fabric ducts and the control thermostats were placed at a medium level. In a real situation, a hood can be added to the evaporator coil in a way that the return air is only driven from the bottom. However, in the present model, the coil was also moved down. As it was mentioned before, the space height is 6.5 m and the fabric ducts are currently installed at 6.0 m height. The new installation height for the air distribution modelling is 3.5 m creating a 3.0 m difference with respect to the floor. This is the minimum space allowed so the system does not interfere with the production and cleaning activities. Fig. 13 shows the model geometry of the air distribution system at a lower level.

Fig. 14 shows the temperature profiles from the relocation of the air distribution system via fabric ducts at different cross sections along the space. With a supply temperature from the air-socks at 7 °C the temperature in the bulk of the space varied between 9.4 and 16.9 °C considering the same measurement points in Fig. 3a. As observed in Fig. 14, the lowest temperatures were obtained at the occupied zone where the temperature difference obtained between the head and knee level was just 0.3 °C in average. The average temperature at the occupied zone was 9.9 °C while the average temperature at ceiling level was 15.9 °C. Modelling results also show that the limiting factor to achieving lower temperatures at the occupied zone is the heat released by the occupants.

Meanwhile, Fig. 15 depicts the modelled velocity distribution at different cross sections along the space. From this figure

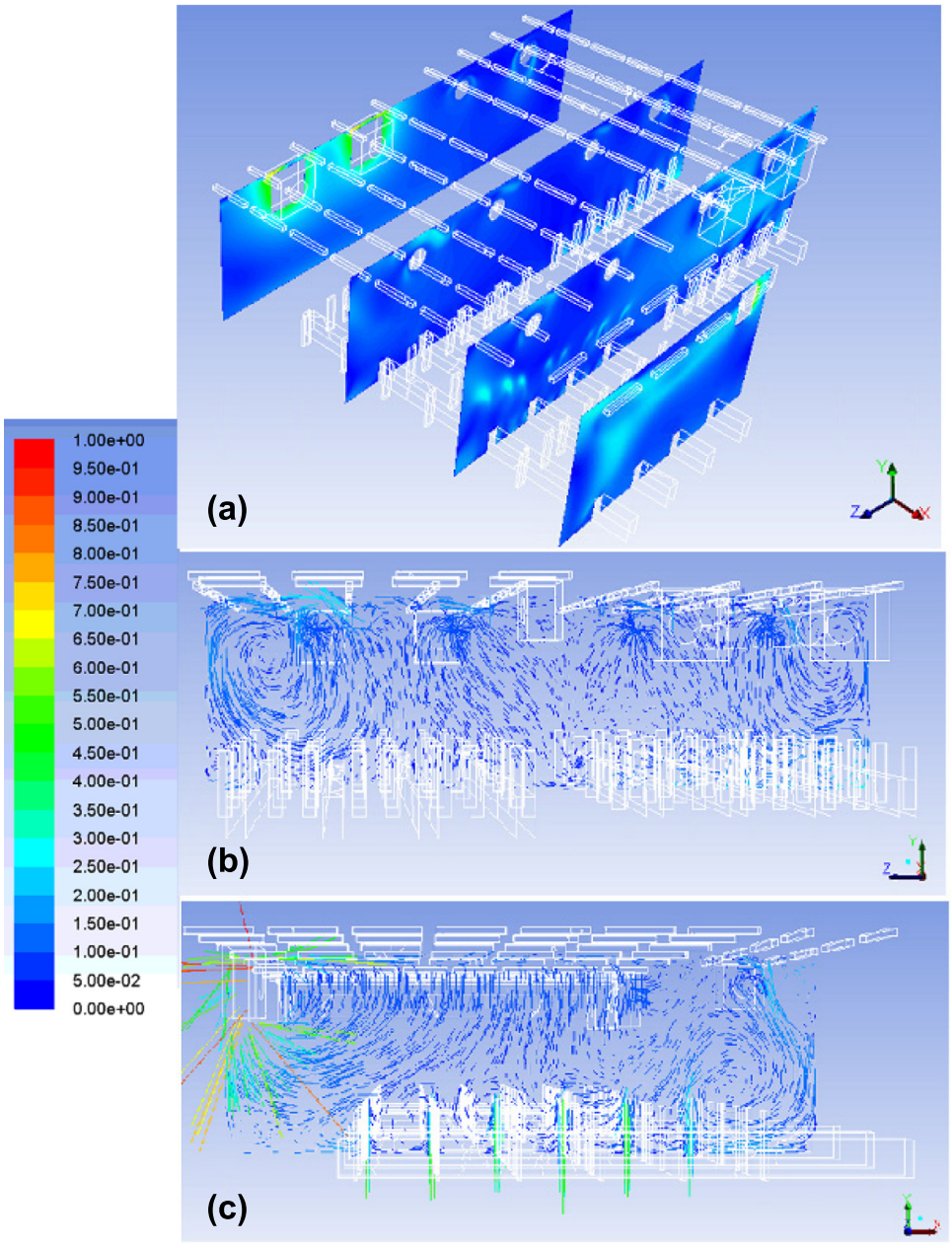

Fig. 11 – Case study 2, CFD modelling of air velocity in the space (m·s^{-1}),(a) 3D view, (b) frontal view, and (c) side view.

it can be observed that the air velocities were similar to the initial model. In this case, velocities varied between 0.02 and 0.35 m·s^{-1}. In Fig. 15 it can also be observed that by locating the air distribution system at a medium level, air displacement is mainly observed at the occupied zone while the air flow at the unoccupied zone is negligible.

Moreover, Fig. 16 presents the comparison between the air temperature profiles obtained from case study 2 and the modified model. The average ceiling level resulting temperatures from the different points of measurement were 11.7 °C and 15.9 °C for the initial and modified configurations, respectively. It means that the predicted air temperatures at ceiling level with the modified model are in average 4.1 °C higher than the initial model. In addition, the average air temperatures at the occupied zone were 10.2 °C and 9.9 °C for the initial and modified configurations, respectively. In total, an average temperature difference was obtained between the unoccupied and occupied zone of 1.5 °C and 5.9 °C for the initial and modified cases, respectively.

In general, it is observed that the temperature difference between the knee and the head level from the modified model is as small as that with the initial model. Furthermore, the modified model results show that the temperature difference between the head and ceiling level is significantly increased when lowering the air distribution system which means that the cold air is localised around the production zone at low air flow velocities. However, it should be a warning that significant temperature difference at ceiling level may result in heat storage at ceiling level which in turn could increase the ceiling temperature and radiative heat exchange with workers in the production area.

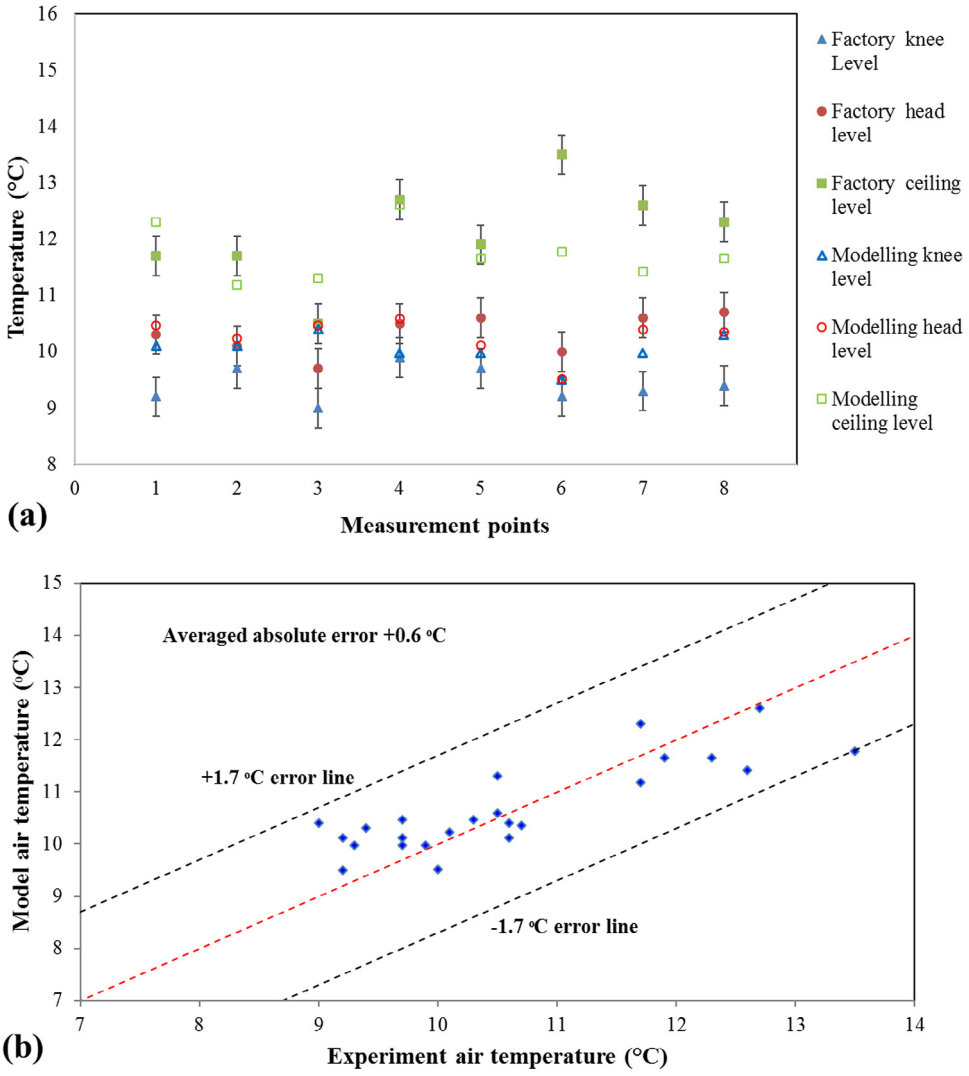

Fig. 12 – Case study 2, (a) air temperature uncertainty analysis and (b) CFD modelling air temperature valuation.

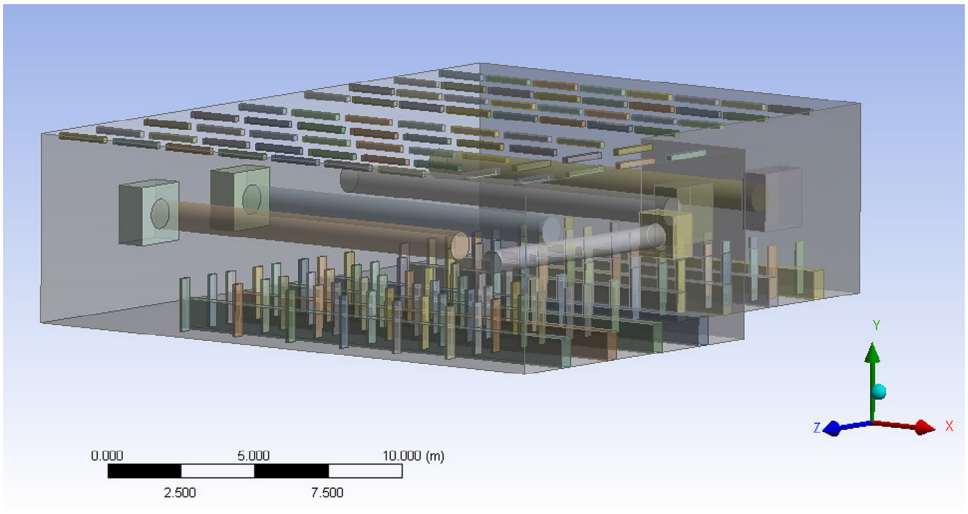

Fig. 13 – Case study 3, fabric ducts at medium level 3D model.

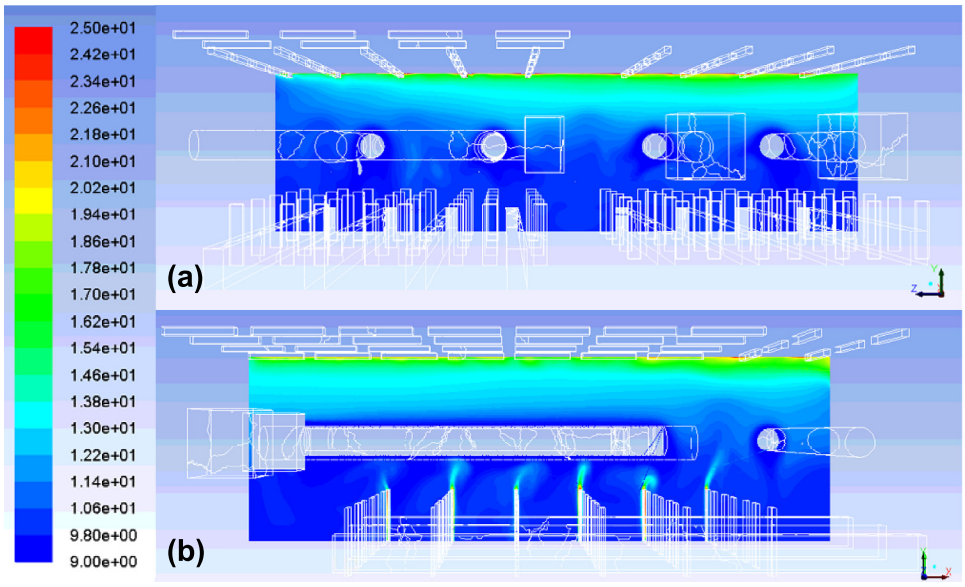

Fig. 14 – Case study 3, CFD modelling of air temperature (°C), cross sections (a) frontal view and (b) side view.

Modelling results demonstrate the feasibility of flexible systems which can be easily retrofitted onto existing air distribution systems and could provide both energy savings and better thermal control conditions in the space through low air velocity supply and thermal stratification.

4. Conclusions

This paper outlines research that aims to investigate and improve the efficiency of air distribution and temperature control systems in chilled food manufacturing facilities. Two different air distribution systems (case 1: supply/return diffusers, and case 2: evaporator coils with fabric ducts) used to provide cooling into the space of two existing food manufacturing facilities were analysed both experimentally and numerically. The following conclusions can be drawn from the present study:

- Validation of the computational models showed good accuracy to predict air flows and thermal environment in both case studies. Maximum errors of 2.2 °C and 1.7 °C were obtained for case 1 and 2, respectively.
- Air distribution via supply/return diffusers in case 1 was effective to maintain the required temperature condition

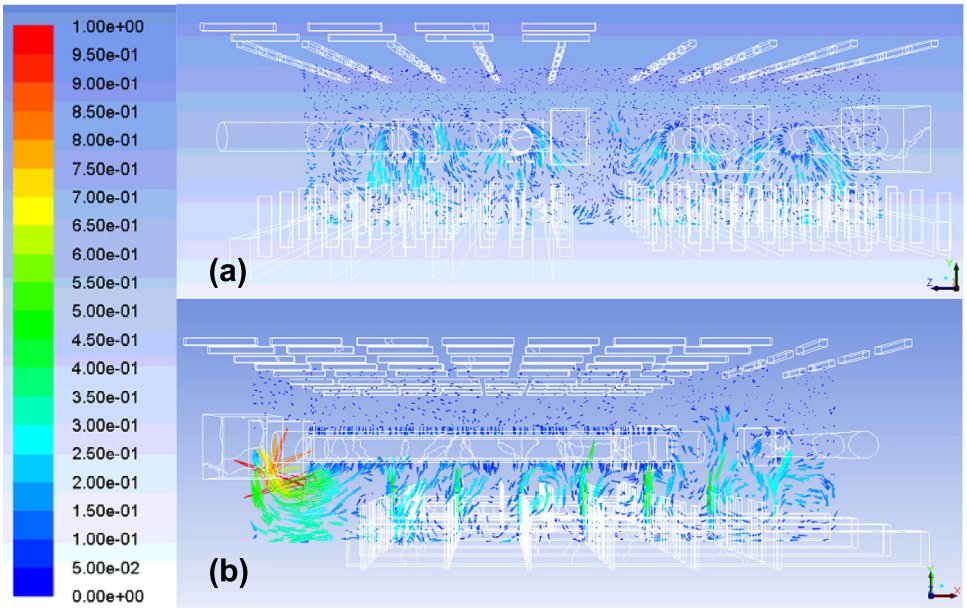

Fig. 15 – Case study 3, CFD modelling of air velocity vectors ($m \cdot s^{-1}$), cross sections (a) frontal view and (b) side view.

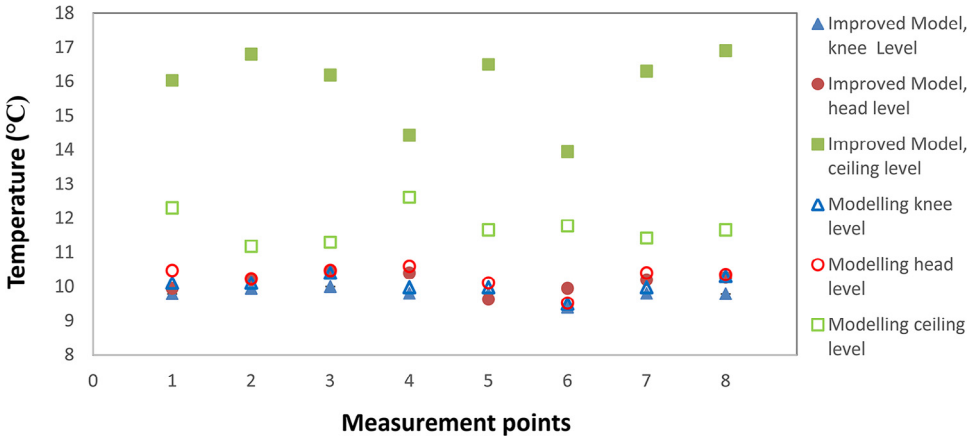

Fig. 16 – Case study 2 vs Case study 3, air temperature distribution.

in the space for maintaining food quality, however, it provided excessive high air flow velocities. In addition, temperature stratification in whole food processing facility space was poor.

- The air distribution system via fabric ducts was found to be a more appropriate method to provide adequate and even air flows, including very low air velocities.
- Further modelling showed that air temperature stratification in the food processing facility can be improved by relocating the fabric ducts at a lower level to localise the coldness around the production zone. It allows maintaining the required temperature around the occupied zone at low air flow velocities and increasing the temperature gradient up to 4.1 °C in the unoccupied zone.
- Future studies will deal with the development of an air flow distribution-energy coupling model to quantify energy savings resulting from the improvement of the air stratification in the space.

Acknowledgments

This project was funded by Innovate UK and the RCUK Centre for Sustainable Energy Use in Food Chains through EPSRC grant No: EP/K011820/1. The authors acknowledge the support from Innovate UK, the RCUK energy programme and contributions from the industrial collaborators Bakkavor and Waterloo Air Products PLC.

REFERENCES

Ambaw, A., Delele, M.A., Defraeye, T., Ho, Q.T., Opara, L.U., Nicolaï, B.M., et al., 2013. The use of CFD to characterize and design post-harvest storage facilities: past, present and future. Comput. Electron. Agric. 93, 184–194.

ANSYS FLUENT Theory Guide, ANSYS, Inc., Release 14.0, Southpointe; 2011.

ASHRAE (American Society of Heating, Refrigerating and Air-Conditioning Engineers), 2013. ASHRAE HANDBOOK, FUNDAMENTALS, Chapter 9.

BS EN ISO 7730, ISO, Ergonomics of the thermal environment – Analytical determination and interpretation of thermal comfort using calculation of the PMV and PPD indices and local thermal comfort criteria;2005.

Chanteloup, V., Mirade, P., 2009. Computational fluid dynamics modelling of local mean age of air distribution in forced-ventilation food plants. J. Food Eng. 90 (1), 90–103.

Cheng, Y., Niu, J., Gao, N., 2012. Stratified air distribution systems in a large lecture theatre: a numerical method to optimize thermal comfort and maximize energy saving. Energy Build. 55, 515–525.

Cheng, Y., Niu, J., Liu, X., Gao, N., 2013. Experimental and numerical investigations on stratified air distribution systems with special configuration: thermal comfort and energy saving. Energy Build. 64, 154–161.

Chourasia, M.K., Goswami, T.K., 2007a. Simulation of effect of stack dimensions and stacking arrangement on cool-down characteristics of potato in a cold store by computational fluid dynamics. Biosyst. Eng. 96 (4), 503–515.

Chourasia, M.K., Goswami, T.K., 2007b. Steady state CFD modeling of airflow, heat transfer and moisture loss in a commercial potato cold store. Int. J. Refrigeration 30 (4), 672–689.

Chourasia, M.K., Goswami, T.K., 2007c. Three dimensional modeling on airflow, heat and mass transfer in partially impermeable enclosure containing agricultural produce during natural convective cooling. Energy Convers. Manag. 48 (7), 2136–2149.

CIBSE (Chartered Institution of Building Services Engineers). Guide A, Environmental design, Appendix 3.A4, Eighth edition; 2015.

Defra (Department of Environment, Food and Rural Affairs). Food Statistics Pocketbook; 2012; 86.

Delele, M.A., Schenk, A., Tijskens, E., Ramon, H., Nicolaï, B.M., Verboven, P., 2009. Optimization of the humidification of cold stores by pressurized water atomizers based on a multiscale CFD model. J. Food Eng. 91 (2), 228–239.

Delele, M.A., Ngcobo, M.E.K., Getahun, S.T., Chen, L., Opara, U.L., 2013. Studying airflow and heat transfer characteristics of a horticultural produce packaging system using a 3-D CFD model. Part I: model development & validation. Postharvest Biol. Technol. 86, 536–545.

Duret, S., Hoang, H.M., Flick, D., Laguerre, O., 2014. Experimental characterization of airflow, heat and mass transfer in a cold room filled with food products. Int. J. Refrigeration 46, 17–25.

Fathollahzadeh, M.H., Heidarinejad, G., Pasdarshahri, H., 2015. Prediction of thermal comfort, IAQ, and energy consumption in a dense occupancy environment with the under floor air distribution, system. Build. Environ. 90, 96–104.
Ho, S.H., Rosario, L., Rahman, M.M., 2010. Numerical simulation of temperature and velocity in a refrigerated warehouse. Int. J. Refrigeration 33 (5), 1015–1025.
Jurelionis, A., Gagyte, L., Prasauskas, T., Ciuzas, D., Krugly, E., Seduikyte, L., et al., 2015. The impact of the air distribution method in ventilated rooms on the aerosol particle dispersion and removal: the experimental approach. Energy Build. 86, 305–313.
Ke-fibertec KE, Low Impulse textile duct fabric. http://www.ke-fibertec.com/uk. (Accessed 28 July 2017).
Laguerre, O., Duret, S., Hoang, H.M., Guillier, L., Flick, D., 2015. Simplified heat transfer modeling in a cold room filled with food products. J. Food Eng. 149, 78–86.
Lin, Y.J.P., Tsai, T.Y., 2014. An experimental study on a full-scale indoor thermal environment using an under-floor air distribution system. Energy Build. 80, 321–330.
Menter, F.R., 1994. Two-equation eddy-viscosity turbulence models for engineering applications. AIAA J 32, 1598–1605.
Moureh, J., Flick, D., 2005. Airflow characteristics within a slot ventilated enclosure. Int. J. Heat Fluid Flow 26, 12–24.
Moureh, J., Tapsoba, M.S., Flick, D., 2009a. Airflow in a slot-ventilated enclosure partially filled with porous boxes: part I – measurements and simulations in the clear region. Comput. Fluids 38, 194–205.
Moureh, J., Tapsoba, S., Derens, E., Flick, D., 2009b. Air velocity characteristics within vented pallets loaded in a refrigerated vehicle with and without air ducts. Int. J. Refrigeration 32, 220–234.
Ning, M., Mengjie, S., Mingyin, C., Dongmei, P., Shiming, D., 2016. Computational fluid dynamics (CFD) modelling of air flow field, mean age of air and CO2 distributions inside a bedroom with different heights of conditioned air supply outlet. Appl. Energy 164, 906–915.
Parpas, D., Amaris, C., Tassou, S.A., 2015. Experimental study and modelling of air distribution systems and temperature control for chilled food factories in a scaled test facility. In Proceedings of the 14th International Conference on Sustainable Energy Technologies, Nottingham, UK, 25 – 27 August, 2015, II, 85–95. (Accessed 2 March 2017).
Parpas, D., Amaris, C., Tassou, S.A., 2017a. Experimental investigation and modelling of thermal environment control of air distribution systems for chilled food manufacturing facilities. Appl. Therm. Eng. 127, 1326–1339.
Parpas, D., Amaris, C., Sun, J., Tsamos, K., Tassou, S., 2017b. Numerical study of air temperature distribution and refrigeration systems coupling for chilled food processing facilities. Energy Procedia 123, 156–163.
Pasut, W., Bauman, F., De Carli, M., 2014. The use of ducts to improve the control of supply air temperature rise in UFAD systems: CFD and lab study. Appl. Energy 134, 490–498.
Rhee, K.-N., Shin, M.-S., Choi, S.-H., 2015. Thermal uniformity in an open plan room with an active chilled beam system and conventional air distribution systems. Energy Build. 93, 236–248.
Smale, N.J., Moureh, J., Cortella, G., 2006. A review of numerical models of airflow in refrigerated food applications. Int. J. Refrigeration 29 (6), 911–930.
Stamou, A., Katsiris, I., 2006. Verification of a CFD model for indoor airflow and heat transfer. Build. Environ. 41, 1171–1181.
Tassou, S.A., Gowreesunker, B.L., Parpas, D., Raeisi, A., 2015. Modelling cold food chain processing and display environments. In: Modelling Food Processing Operations. Elsevier, pp. 185–208. ISBN-139781782422846.
Zhang, K., Zhang, X., Li, S., 2016. Simplified model for desired airflow rate in underfloor air distribution (UFAD) systems. Appl. Therm. Eng. 93, 244–250.